Proceedings of the 16th International Conference on Soil Mechanics and Geotechnical Engineering

doi:10.3233/978-1-61499-656-9-933

Soil-water coupled elasto-plastic analysis on bearing capacity of naturally deposited clay soil

Analyse élasto-plastique couplée sol-eau sur la capacité portante du sol en argile par dépôt naturel

T. Noda
Nagoya University, Japan
S. Yamada
Kyushu University, Japan

ABSTRACT
To investigate a problem of bearing capacity of a natural clay, a soil-water coupled finite deformation analysis is performed with the elasto-plastic constitutive model that describes the effect of the decay of soil skeleton structure due to plastic deformation. From the computational results the findings are as follows: (1) In a structured clay soil, a load peak phenomenon appears, accompanied by a local circular slip field. (2) In a clay soil possessing anisotropy, this area of failure is more confined, and the peak is lower.

RÉSUMÉ
Le problème de la capacité portante de fondations en argile par dépôt naturel est étudié par l'exécution d'une analyse de déformation finie couplée eau-sol par un modèle constitutif élasto-plastique décrivant les effets de l'altération du squelette de la structure du sol résultant de la déformation plastique. Les résultats des calculs montrent que : (1) Dans du sol de structure se produit un phénomène de pointe de charge accompagné d'un champ d'éboulement circulaire local ; (2) Dans du sol avec anisotropie, cette zone de défaillance est plus réduite et la pointe moins accentuée.

1 INTRODUCTION

Stability problems in naturally deposited clay soil, such as those containing soft clay, can be analyzed using limit bearing capacity analysis methods such as a ϕ_u=0 circular slip analysis or a soil-water coupled (Asaoka et al., 1990) rigid plastic finite element analysis (Tamura et al., 1984). Using the latter method, it is an easy matter, having first found the void ratio distributions in the soil through an elasto-plastic consolidation deformation analysis under partially drained conditions, to project them over into the rigid plastic analysis in order to obtain the bearing capacity ('partially drained bearing capacity analysis' (Asaoka et al., 1990)). More recently, however, it has become possible to tackle this kind of bearing capacity problem within a single theoretical framework, while still taking account of the change in geometrical shape, by making use of a soil-water coupled elasto-plastic finite deformation analysis that is able to deal with the whole sequence of change from deformation through to failure (Asaoka et al., 1994). To grasp the initial state of the soil for an elasto-plastic analysis of this sort, it is vital to have access to an elasto-plastic model that can describe not only the void ratio distributions, as required for a rigid plastic analysis, but also other information relevant to a naturally deposited clay soil, such as the degree of soil structure and any subsequent changes in the soil skeleton.

In this paper we report a soil-water coupled finite deformation calculation (Asaoka et al., 1994) of the bearing capacity of a naturally deposited and highly structured clay soil, performed using an elasto-plastic model that describes the soil skeletal mechanisms of structure, overconsolidation and anisotropy (Asaoka et al., 2000, 2002). We then discuss the influence that soil structure and anisotropy have on the calculated bearing capacity, the influence of the initial imperfection in geometrical shape, and the influence played by the loading rate, through its effect on the soil-water coupling. To enable the bearing capacity problem to be presented in an easily understandable classical form, it will be supposed that the foundation is to be rigid, thin, and controlled in its vertical displacement.

2 ELASTO-PLASTIC CONSTITUTIVE EQUATION FOR NATURAL CLAY

2.1 *The quantitative expression of structure, overconsolidation and anisotropy, and their evolution rules*

Naturally deposited soils, whether clayey or sandy, generally exist in an overconsolidated structured state. A necessary base for describing the deformational behavior of soils in this state is an elasto-plastic model of a soil that has been deprived of its structure through remolding and returned to a state of normal consolidation. However, even an unstructured and normally consolidated soil possesses isotropy, and therefore this paper also makes use of a stress parameter η^* by Sekiguchi and Ohta (1977) and the associated evolutionary concept of rotational hardening (Hashiguchi & Chen, 1998) first introduced into the Cam-clay model to provide an expression of anisotropy. The two further concepts of a superloading (Asaoka et al., 2000) and of a subloading (Hashiguchi, 1989) yield surface, are added to this revised model to allow the expression and quantification of degrees of structure and overconsolidation, respectively. The degree of structure is expressed on a superloading surface, similar to the Cam-clay yield surface but situated outside it (similarity ratio R^* defined: $0 < R^* \leq 1$ at center of similarity $p' = q = 0$) , while the state of overconsolidation is expressed on a subloading surface inside the superloading one (similarity ratio R defined: ($0 < R \leq 1$) at center of similarity $p' = q = 0$; the reciprocal, $1/R$ is thus equivalent to the overconsolidation ratio). Here, p' is the mean effective stress and q is the shear stress, given as $p' = -\mathrm{tr}\boldsymbol{T}'/3$ and $q = \sqrt{3/2}\,\boldsymbol{S}\cdot\boldsymbol{S}$ for effective stress tensor $\boldsymbol{T}'$ (tension: positive). The closer R^* comes to 0, the higher the degree of structure; but an increase in plastic deformation brings loss of structure meaning that R^* approaches 1 (evolution rule for R^*). Similarly, the closer R is to 0, the higher the degree of overconsolidation; but as R increases with plastic deformation and comes closer to 1, the soil also comes closer to the state of normal consolidation (evolution rule for R). It can therefore be presumed that any advance in plastic deformation will result in a simultaneous loss of structure and of overconsolidation (a movement toward the normally consolidated state), leading ultimately to the conditions assumed in the Cam-clay model. If the three yield surfaces are imagined placed

in axi-symmetry on a set of coordinates, we obtain the arrangement in Fig. 1. As the current effective stress is situated on the subloading yield surface, the various elasto-plastic principles such as the associated flow rule and Prager's consistency condition are applied to the subloading surface represented by

$$f(p',\eta^*) + \mathrm{MD}\ln R^* - \mathrm{MD}\ln R + \int_0^\tau J\mathrm{tr}\boldsymbol{D}^p d\tau = \mathrm{MD}\ln\frac{p'}{p'_0} + \mathrm{MD}\ln\frac{\mathrm{M}^2+\eta^{*2}}{\mathrm{M}^2} + \mathrm{MD}\ln\frac{R^*}{R} + \int_0^\tau J\mathrm{tr}\boldsymbol{D}^p d\tau = 0 \quad (1)$$

Here, $\mathrm{D} = (\tilde{\lambda}-\tilde{\kappa})/\mathrm{M}/(1+\mathrm{e}_0)$ is the dilatancy coefficient, M is the critical state constant, $\tilde{\lambda}$ and $\tilde{\kappa}$ are the compression and swelling indices, and e_0 is the initial void ratio where $J=(1+\mathrm{e})/(1+\mathrm{e}_0)$ (e is the void ratio at time t = t). $\boldsymbol{D}^p$ is the plastic stretching tensor and $-\int_0^\tau J\mathrm{tr}\boldsymbol{D}^p d\tau$ (compression: positive) corresponds to the plastic volumetric strain. Anisotropy, represented by η^*, can be expressed in terms of the effective stress and the rotational hardening tensor $\boldsymbol{\beta}$, as following, $\eta^* = \sqrt{3/2}\,\hat{\boldsymbol{\eta}}\cdot\hat{\boldsymbol{\eta}}$, $\hat{\boldsymbol{\eta}} = \boldsymbol{\eta}-\boldsymbol{\beta}$, $\boldsymbol{\eta} = \boldsymbol{S}/p'$ and $\boldsymbol{S} = \boldsymbol{T}'+p'\boldsymbol{I}$. For the purposes of this paper, the evolution rules for R^*, R and $\boldsymbol{\beta}$ are given by the following Eqs. (2) – (4).

$$\dot{R}^* = JU^*\left\|\boldsymbol{D}^p\right\|,\ U^* = \frac{a}{\mathrm{D}}R^{*b}(1-R^*)^c \quad (2)$$

$$\dot{R} = JU\left\|\boldsymbol{D}^p\right\|,\ U = -\frac{m}{\mathrm{D}}\ln R \quad (3)$$

$$\overset{\circ}{\boldsymbol{\beta}} = J\frac{br}{\mathrm{D}}\sqrt{\frac{2}{3}}\left\|\boldsymbol{D}_s^p\right\|\left\|\hat{\boldsymbol{\eta}}\right\|\left(m_b\frac{\hat{\boldsymbol{\eta}}}{\left\|\hat{\boldsymbol{\eta}}\right\|}-\boldsymbol{\beta}\right) \quad (4)$$

$\boldsymbol{D}_s^p$ is the deviator component of $\boldsymbol{D}^p$ and the $\|\ \|$ terms show the respective norms. $\boldsymbol{\beta}$ in Eq. (4) is the Green & Naghdi's (1965) rate of $\boldsymbol{\beta}$. The groups of parameters in all three equations consist wholly of constants. From the point of view of the roles they perform, *a*, *b* and *c* are degradation indices of structure, *m* is a degradation (or loss) index of overconsolidation, b_r is an evolution index of rotational hardening, and m_b is a rotational hardening limit. As for the values of these evolution parameters, a comparison of responses obtained from the constitutive equation and from laboratory experiments shows categorically that, compared with sand, clay has a slower rate of evolution for structural degradation and anisotropy, and a faster rate for loss of overconsolidation (Asaoka et al., 2002).

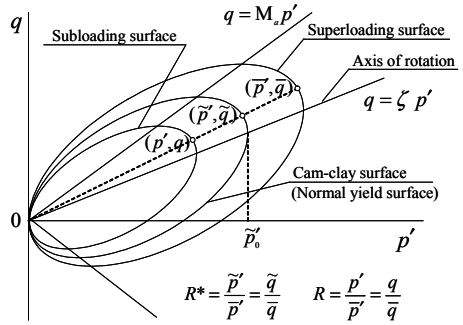

Figure 1. The three loading surfaces.

2.2 The associated flow rule and the constitutive equation

Associated flow rule:

$$\boldsymbol{D}^p = \lambda\frac{\partial f}{\partial \boldsymbol{T}'},\ \lambda = \frac{\frac{\partial f}{\partial \boldsymbol{T}'}\cdot\overset{\circ}{\boldsymbol{T}}'}{J\frac{\mathrm{MD}}{p'(\mathrm{M}^2+\eta^{*2})}(\mathrm{M}_s^{\ 2}-\eta^2)} > 0 \quad (5)$$

Constitutive equation: $\overset{\circ}{\boldsymbol{T}}' = \boldsymbol{E}\boldsymbol{D} - \Lambda\boldsymbol{E}\frac{\partial f}{\partial \boldsymbol{T}'}$ (6)

$\boldsymbol{E}$ is the elastic tensor, $\overset{\circ}{\boldsymbol{T}}'$ is the Green & Naghdi's rate of $\boldsymbol{T}'$, and Λ expresses the plastic multiplier λ under stretching $\boldsymbol{D}$. Further,

$$\mathrm{M}_s^{\ 2} = \mathrm{M}_a^{\ 2} + b_r\frac{4\mathrm{M}\eta^{*2}}{\mathrm{M}^2+\eta^{*2}}(m_b\eta^* - \sqrt{\frac{3}{2}}\hat{\boldsymbol{\eta}}\cdot\boldsymbol{\beta}) - \mathrm{MD}\left(\frac{U^*}{R^*}-\frac{U}{R}\right)\sqrt{6\eta^{*2}+\frac{1}{3}(\mathrm{M}_a^{\ 2}-\eta^2)^2} \quad (7)$$

where a relation obtains of $\mathrm{M}_a^{\ 2} = \mathrm{M}^2 + \zeta^2$, $\zeta = \sqrt{3/2}\|\boldsymbol{\beta}\|$. For details of this, the reader is referred to Asaoka et al.(2002), but the essential point is that the slope M_s of the threshold between hardening and softening $q = \mathrm{M}_s p'$, under the loading condition $\lambda > 0$, varies wildly with structural degradation, loss of overconsolidation and gain or loss of anisotropy, as well as with current stress; also, the slope M_a of the threshold between plastic compression and expansion $q = \mathrm{M}_a p'$ varies in response to the gain or loss of anisotropy.

3 THE BEARING CAPACITY OF A NATURALLY DEPOSITED CLAY SOIL

3.1 *Calculation conditions*

The calculation is performed for 2-dimensional plane strain conditions, using the finite element mesh and boundary conditions shown in Fig. 2. A foundation is assumed to be rigid and possessing friction. Since it is possible for the foundation to have an asymmetrically deformed mode allowing a tilt to one side by making use of a whole cross-section, restrictions on line shape (invariability of length and angle) (Asaoka et al., 1998) will be imposed between nodes. In order not to cause no more than a minimal migration of pore water inside the soil, forced vertical displacements are assumed to be applied in a downward direction at the central node of the base, at a high velocity of 10^{-5} cm/sec.

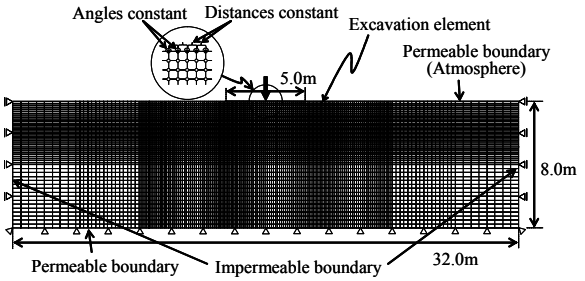

Figure 2. Finite element mesh and boundary conditions.

Table 1 shows the material constants. The values for the evolution rule parameters are fixed so as to capture the typical elasto-plastic behaviors of clay (slow decay of structure and gain in anisotropy, rapid loss of overconsolidation)(Asaoka et al., 2002). The initial distributions of the void ratios and degrees of structure in the soil can then be determined as follows, taking account of the soil's own weight. First the constitutive equation is used to find theoretical 1-dimensional values for a horizontally homogeneous normally consolidated soil state under the action of a surcharge load of 98.1 kPa plus gravity, and the consolidation after the removal of the surcharge load is calculated. The bearing capacity is then calculated for the somewhat overconsolidated state of the soil without the surcharge load. As actual initial state values in the soil at the normally consolidated stage will depend on conditions that vary on part from case to

case in the calculated results presented below, let us begin by discussing this point before looking at individual calculations. The fact that the weight of the soil particle itself has to be allowed for in the balance of forces problem, and that account has to be taken of the associated increase in strength (non-homogeneity) which appears at lower depths in the soil, means that the bearing capacity has to be treated in a quite different way from what would be usual in metal plasticity theory.

Table 1. Material constants in the clay.

Elasto-plastic parameters	
Compression index $\tilde{\lambda}$	0.23
Swelling index $\tilde{\kappa}$	0.01
Critical state constant M	1.15
Specific volume at $q = 0$ and $p' = 98.1$ kPa on NCL N	2.75
Poisson's ratio ν	0.1
Evolution rule parameters	
Degradation index of structure a ($b = c = 1.0$)	0.2
Degradation index of overconsolidation m	5.0
Evolution index of rotational hardening b_r	0.001
Limit of rotational hardening m_b	1.0
Permeability k (cm/sec)	2.8×10^{-8}
Density of soil particle ρ_s (t/m^3)	2.75

3.2 *lculation results (influence of presence or absence of structure)*

We now compare the initial degrees of structure in the soil. Table 2 gives the initial conditions in the highly and less structured soils before the removal of the surcharge load, while Fig. 3 shows the various distributions in both the soils after unloading and consolidation and just prior to loading. The calculation results are shown in Figs. 4 (settlement-to-load relation) and 5 (comparison of distribution of shear strain). In the case of the less structured soil (i.e., remolded soil), the settlement proceeds continuously together with the increase in the added load. Even though an exhaustion of elasticity and a change to plastic behavior may appear at the element level as shown below, this ongoing growth comes from the fact that we are dealing here with the moment by moment geometrical change in shape in the soil as a whole, a case quite different from that of a limit analysis based on rigid plasticity theory. In fact we find the soil horizontally next to the foundation of the soil rising to function as a "counterweight fill" as the loading increases. In a highly structured clay, on the other hand, the scope of the analysis will effectively be confined to occurrences of "slip" in the immediate vicinity of the foundation. In cases where softening behavior appears at the element level, this will tend to be offset by the effect of geometrical shape changing, so that the loading shows a peak followed by a fresh phase of rising to follow. While the conditions described are different, it may be added that the area of slip obtained here is more restricted than that by Prandtl. Fig. 6 shows the comparison of the behavior on the shear localized area. The structured clay displays softening due to the structural decay after hardening due to the overconsolidation loss, while the remolded clay displays a near-perfectly plastic behavior.

Table 2. Initial conditions in the soils.

Elasto-plastic parameters	Highly structured	Less structured
Degree of structure R_0 *	0.25	1.0
Overconsolidation ratio $1/R_0$	1.0	1.0
Lateral pressure coefficient $\sigma_{h0}'/\sigma_{v0}'$	0.5	0.5
Degree of anisotropy $\zeta_0 = \sqrt{3/2}\beta_0 \cdot \beta_0$	0.75	0.75

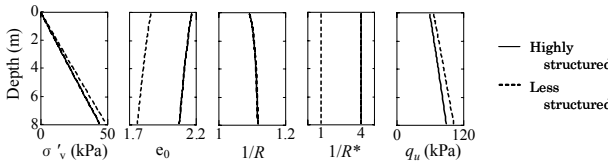

Figure 3. Initial distributions (q_u: undrained strength).

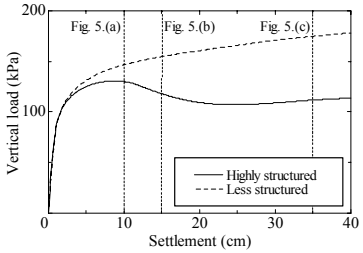

Figure 4. Influence of structure (settlement in relation to load).

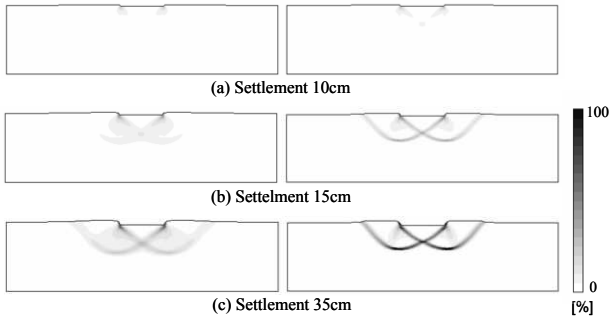

Figure 5. Influence of structure (distribution of shear strain).

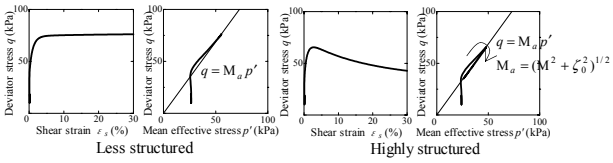

Figure 6. Clay element behavior on shear localized area.

3.3 *Calculation results (influence of anisotropy)*

In a natural soil with a well developed soil skeleton structure it is common, also, for anisotropy to be highly developed. Starting each time from the same initial anisotropy stress state shown in Table 2, a comparison has been made between states with and without initial anisotropy(initial yield surface inclined as in Fig. 1; isotropic when $\zeta_0 = \sqrt{3/2}\|\boldsymbol{\beta}_0\| = 0$; anisotropic when $\zeta_0 \neq 0$). The results are shown in Figs. 7 (settlement-to-load) and 8 (comparison of distribution of shear strain). Clearly, in a soil with prominent initial anisotropy the peak load and the size of the "circular slip" area are both smaller. Remarkably, this conclusion does not differ in any respect from one arrived at more than ten years ago through an analysis based on rigid plasticity theory (Asaoka & Kodaka, 1992).

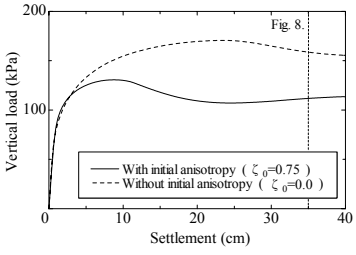

Figure 7. Influence of initial anisotropy (settlement to load).

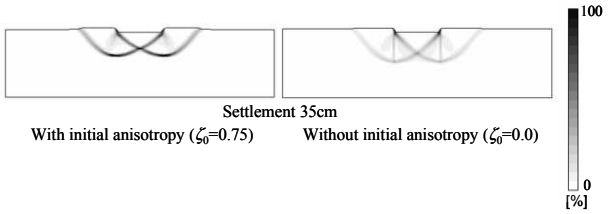

Figure 8. Influence of initial anisotropy (distribution of shear strain).

3.4 *Calculation results (influence of initial imperfection in geometrical shape of the soil)*

The results reported in 3.2 and 3.3 were for the analysis of a whole cross-section without any initial imperfection in geometrical shape. Figs. 9 (displacement-to-load) and 10 (comparison of distribution of shear strain) show results calculated for a whole cross-section with an initial imperfection. The imperfection was created by removing a finite element from the mesh with no imperfection as shown in Fig. 2, followed by performing a calculation of consolidation prior to loading. The other calculation conditions remain the same as in Table 2. When the mesh with the imperfection is applied the deformation proceeds asymmetrically, "bifurcating" from the "true path" at one point and becoming smaller. Some initial imperfection should be incorporated in the real state of things, whether geometrical or material in origin. Therefore, an asymmetrical mode breakdown of the kind shown in Fig. 10 will always be close to the reality.

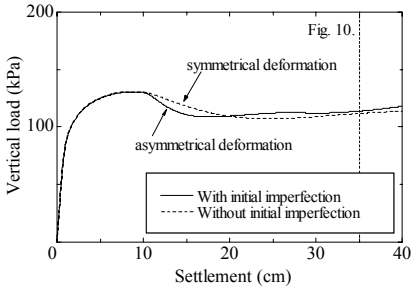

Figure 9. Influence of initial imperfection in geometrical shape (settlement in relation to load).

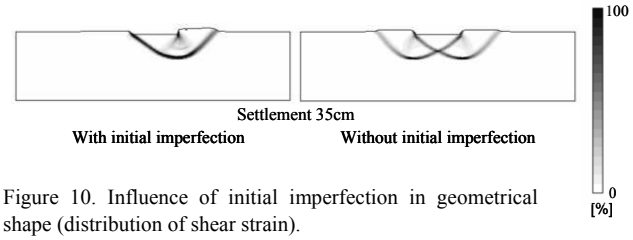

Figure 10. Influence of initial imperfection in geometrical shape (distribution of shear strain).

3.5 *Calculation results (influence of loading rate)*

The above results are all for rapid loading (≅ completely undrained). But in order to show the effect of a soil-water coupled calculation, it is necessary to say something about the effect of partial drainage. Accordingly, calculations have been performed for forced vertical displacement velocities set at 10^{-5} and 10^{-6}cm/sec. The initial conditions are the same as in Table 2 (Highly structured). The results are given in Figs. 11 (settlement-to-load) and 12 (specific volume change distribution). Fig. 12 shows the area around the so-called "slip line," and is of importance in that it is possible to see the swelling or compression of the soil. At a lower loading rate, compression (a compaction band) becomes visible in the vicinity of the localization area of the shear strain (the slip line).

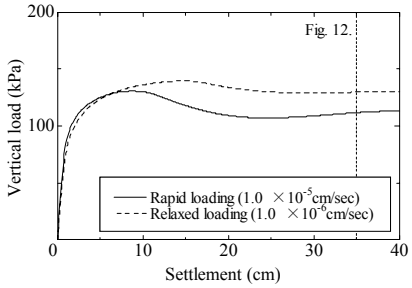

Figure 11. Influence of loading rate (settlement in relation to load).

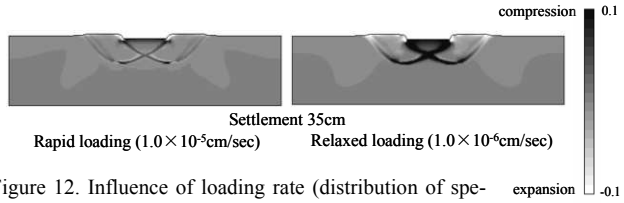

Figure 12. Influence of loading rate (distribution of specific volume change from initial state).

4 CONCLUSION

With a focus on a problem of bearing capacity, this paper has reported a soil-water coupled finite deformation analysis performed with an elasto-plastic model describing the working of soil skeleton structure, and has shown among other things that (1) in a structured soil, a load peak phenomenon appears, accompanied by a local circular slip field (area of failure) (Figs. 4 and 5); (2) in a soil possessing anisotropy, this area of failure is more confined, and the peak is lower (Figs. 7 and 8); (3) in a structured soil with an initial imperfection in geometrical shape, an imperfection-sensitive behavior appears (Figs. 9 and 10); and (4) at lower loading rates a compaction band becomes visible (Figs. 11 and 12). Lack of page space has made it impossible to deal with the influences due to overconsolidation, but it should now be apparent that the scope of the problem areas that can be treated in an analysis of this kind is very broad, and that the inclusion of the soil structure concept and of anisotropy here is as natural as it is important, since both are characteristic features of a naturally deposited soil. On the subject of bearing capacity in conditions of embankment loading – i.e. under controlled weight loads –, the authors report elsewhere(Asaoka et al., 2005).

REFERENCES

Asaoka, A., Ohtsuka, S. and Matsuo, M. 1990. Coupling analysis of limiting equilibrium state for normally consolidated and lightly overconsolidated soils, *Soils and Foundations*, 30(3), 109-123.

Asaoka, A. and Kodaka, T. 1992. Bearing capacity of foundations on clays by the rigid plastic finite element model, *Proc. 4th Int. Symp. Num. Models Geomech.-NUMOG IV*, 839-849.

Asaoka, A., Nakano, M. and Noda, T. 1994. Soil-water coupled behaviour of saturated clay near/at critical state, *Soils and Foundations*, 34(1), 91-106.

Asaoka, A., Noda, T., Yamada, E. and Tashiro, M. 2005. Progressive consolidation of highly structured clay under embankment loading, to appear in the present international conference.

Asaoka, A., Noda, T. and Kaneda, K. 1998. Displacement/traction boundary conditions represented by constraint conditions on velocity field of soil, *Soils and Foundations*, 38(4), 173-181.

Asaoka, A., Nakano, M. and Noda, T. 2000. Superloading yield surface concept for highly structured soil behavior, *Soils and Foundations*, 40(2), 99-110.

Asaoka, A., Noda, T., Yamada, E., Kaneda, K. and Nakano, M. 2002. An elasto-plastic description of two distinct volume change mechanisms of soils, *Soils and Foundations*, 42(5), 47-57.

Green, A.E. and Naghdi, P.M. 1965. A general theory of an elastic-plastic continuum, *Arch. Rat. Mech. and Analy.*, 18, 251-281.

Hashiguchi, K. and Chen, Z. P. 1998. Elastoplastic constitutive equations of soils with the subloading surface and the rotational hardening, *Int. J. Num. Anal. Meth. Geomech.* 22, 197-227.

Hashiguchi, K. 1989. Subloading surface model in unconventional plasticity, *Int. J. of Solids and Structures* 25, 917-945.

Sekiguchi, H. and Ohta H. 1977. Induced anisotropy and time dependency in clays, *Constitutive Equations of Soils* (*Proc. 9th Int. Conf. Soil Mech. Found. Eng., Spec. Session 9*), Tokyo, 229-238.

Tamura, T., Kobayashi, S. and Sumi, T. 1984. Limit analysis of soil structure by rigid plastic finite element method, *Soils and Foundations*, 24(1), 34-42.